New phosphorescent iridium(III) dipyrrinato complexes: synthesis, emission properties and their deep red to near-infrared OLEDs

Hongyang Zhang,[a,b,c] Haitao Wang,[c] Kevin Tanner,[d] Adrien Schlachter,[d] Zhao Chen,*[,e] Pierre D. Harvey,*[,d] Shuming Chen,*[,f] Wai-Yeung Wong*[,a,b,c]

A series of heteroleptic Ir(III) complexes composed of two cyclometalated C^N ligands and one dipyrrinato ligand used as an ancillary ligand are synthesized and characterized. With the introduction of a fluorine atom, phenyl ring or diphenylamino group onto both C^N ligands and by keeping the ancillary ligand unchanged, these Ir(III) dipyrrinato phosphors do not show an obvious shift on their emission bands. They exhibit emissions extending well in the near-infrared region with an intense band located at around 685 nm in both photo- and electroluminescence spectra, and the deep red to near-infrared organic light emitting diodes (OLEDs) based on them afforded a maximum external quantum efficiency of 2.8%. Density functional theory (DFT) calculations show that both the distribution of the atomic contributions on the lowest unoccupied molecular orbitals (LUMOs) and the highest energy semi-occupied molecular orbitals (HSOMOs) are mainly localized on the dipyrrinato ligand, indicating that the ancillary ligand, which remains unchanged in this series, exhibits a lower triplet state energy in the iridium phosphors than those involving the C^N ligands. Therefore a switch from "(C^N)2Ir" to dipyrrinato-based emission is observed in these iridium(III) complexes.

[a] *Department of Applied Biology and Chemical Technology, The Hong Kong Polytechnic University (PolyU), Hong Kong, China. E-mail: wai-yeung.wong@polyu.edu.hk*
[b] *PolyU Shenzhen Research Institute, Shenzhen 518057, China.*
[c] *Department of Chemistry, Hong Kong Baptist University, Waterloo Road, Hong Kong, China.*
[d] *Département de Chimie, Université de Sherbrooke 2550 Boulevard Université, Sherbrooke, PQ, Canada, J1K 2R1. E-mail: Pierre.Harvey@USherbrooke.ca*
[e] *School of Applied Physics and Materials, Wuyi University, Jiangmen 529020, China. E-mail: chenzhao2006@163.com*
[f] *Department of Electrical and Electronic Engineering, Southern University of Science and Technology, Shenzhen 518000, China. E-mail: chensm@sustech.edu.cn*

Introduction

Transition metal ions, such as Fe(II),[1,2,3] Ru(II),[4,5] Os(II),[6,7] Co(III),[8,9,10] Rh(III)[11,12] and Ir(III)[13,14] adopt octahedral coordination geometry with the d^6 electronic configuration, in which the metal center is connected with the ligands through six coordination bonds. Among them, Ru(II), Os(II), Rh(III) and Ir(III) complexes have been demonstrated to be triplet emitters due to the strong spin-orbit coupling of the heavy atom, which promotes the intersystem crossing (ISC) from the upper singlet excited states to the triplet excited states, therefore ultimately populating the lowest energy triplet excited state (T_1).[15,16,17] The cyclometalated Ir(III) complexes show high efficiency of intersystem crossing compared with other metal complexes as witnessed by the relatively short lifetime of their triplet states. Thus, cyclometalated Ir(III) complexes have been widely used in phosphorescent OLEDs.[13,14,16,18,19,20] According to the variety of cyclometalated ligands reported in the literature, the Ir(III) phosphors can be divided into homoleptic[18] and heteroleptic[19] complexes. It is worth noting that heteroleptic Ir(III) complexes composed of two bidentate C^N ligands and one ancillary ligand are some of the most investigated systems.[21] The photophysical and electrochemical properties of the Ir(III) complexes are prone to be tuned by employing different cyclometalated ligands that can regulate the HOMO and LUMO energy levels via the coordination to the metal orbitals.[17,18,19,21,22] It has been demonstrated that introducing the conjugated groups and/or electron-donating groups into the cyclometalated ligands would expectedly red shift the emission band (known as bathochromic effect), in which the introduction of conjugated groups into the ligands can normally lower the energy of the LUMO levels of Ir(III) complexes while incorporating electron-donating group can elevate that of the HOMO levels.[14,22,23]

As the porphyrin precursors, dipyrrinato ligands have attracted increased attention because of their remarkable photophysical properties.[24] Indeed, many boron difluoride (BF_2) dipyrrinato complexes exhibit advanced optical performances owing to their highly absorptive and strongly luminescent characters. Moreover, due to their biocompatibility, these optical features make them good candidate materials for biological labels and sensors.[25] On the other hand, metal dipyrrinato complexes also display rich optoelectronic properties. For example, dipyrrinato zinc(II) complexes show fluorescent quantum yield as high as 0.76 in

toluene.[26] New dipyrrinato fluorescent complexes with green luminescence were reported using group 13 metal ions, gallium(III) and indium(III).[27] In order to improve the relatively low emission efficiencies of homoleptic dipyrrinato In(III) complexes, a series of heteroleptic In(III) complexes bearing various tris(dipyrrinato) ligands was designed and synthesized. One of the complexes exhibits a high fluorescence quantum yield (QY = 0.41 in toluene), exceeding the QY value of the corresponding BF_2 complex.[28] Besides, group 8 to 10 metal ions are also capable of combining with dipyrrinato ligands to afford functional organometallic materials. Homoleptic Co(III)/Fe(III) tris(dipyrrinato) complexes as well as heteroleptic Ni(II)/Pd(II) bis(dipyrrinato) complexes were prepared, in which they can be functionalized as the bridging component to form the dual-metallic metal-organic frameworks (MOFs)[29] and applied as selective chromogenic probes, respectively.[30] Cyclometalated Pt(II) complexes coordinated by dipyrrin-based ligands were synthesized and they exhibit near-infrared (NIR) emission.[31] Ru(II) complexes bearing dipyrrinato, terpyridine and NCS^- ligands were also reported, and these complexes show intense light-absorbing properties in the visible region and can be used as photosensitive dyes in dye-sensitized solar cell (DSSC).[32] Additionally, dipyrrinato ligands can combine with group 7 rhenium(I)[33], group 11 copper(I)[34], even main-group Al(III)[35] and silicon(IV)[36] to form the illuminant agents.[37]

However, the investigations on Ir(III) dipyrrinato complexes are limited.[38,39] We now describe the syntheses and characterizations of a series of tris-bidentate and heteroleptic Ir(III) complexes where a dipyrrinato (**pdp**) ligand is used as the ancillary ligand. This study allows for a comparison with the corresponding Ir(III) complexes using acetylacetonato (**acac**) ligand as the ancillary ligand. To our surprise, these Ir(III) dipyrrinato complexes exhibit little or no variation of the emission colors when the substituents on the cyclometalated ligands are changed. Specifically, with the introduction of conjugated and/or electron-donating groups into the cyclometalated C^N ligands and by keeping the ancillary ligand unchanged, the emission bands of complexes did not significantly shift to the longer wavelengths. Notably, the high semi-occupied molecular orbital, HSOMO, of the dipyrrinato ligand plays a major role on the nature of the triplet emission of the Ir(III) complexes. According to the DFT calculations, the triplet state energy of the dipyrrinato-based manifold is more stable than that of the C^N ligand, thus the T_1 states of all Ir(III) dipyrrinato complexes mostly involve the dipyrrinato ligand. Furthermore, the OLEDs built with these Ir(III) dipyrrinato phosphors display electroluminescent peaks at about 685 nm with a maximum external quantum efficiency (EQE) up to 2.8%.

Results and discussion

Synthetic strategies and chemical characterization

The C^N ligand **piq-dpa** was synthesized in one step through a Suzuki coupling of 1-chloroisoquinoline with 4-(diphenylamino)phenylboronic acid. The other three C^N ligands (**dfppy, ppy, piq**) were obtained from a commercial source. It is worth noting that the use of fluorine atoms on the cyclometalated ligand is the most common way to obtain well-isolated HOMO and LUMO manifolds from the other MOs associated with the remainder of the organometallic complexes. The quinolyl unit bears more conjugated rings compared to phenyl group, which lowers the LUMO level. Concurrently, the electron-donating diphenylamino group destabilizes the HOMO level. The ancillary ligand **pdp** was prepared via the same synthetic route as for the dipyrrin and its derivatives. Then, the metalation of the corresponding cyclometalated C^N ligands with $IrCl_3 \cdot nH_2O$ yielded the colored cyclometalated Ir(III) μ-chloro-bridged dimers. The μ-chloro-bridged dimers were then converted into the desired Ir(III) complexes **Ir(dfppy)$_2$(pdp)** (**Ir1**), **Ir(ppy)$_2$(pdp)** (**Ir2**), **Ir(piq)$_2$(pdp)** (**Ir3**) and **Ir(piq-dpa)$_2$(pdp)** (**Ir4**) by mixing with the dipyrrinato ligand in the presence of sodium carbonate. In comparison, the Ir(III) complexes **Ir(dfppy)$_2$(acac)** (**Ir5**), **Ir(ppy)$_2$(acac)** (**Ir6**), **Ir(piq)$_2$(acac)** (**Ir7**) and **Ir(piq-dpa)$_2$(acac)** (**Ir8**) were synthesized also using dimers, which reacted with acetylacetone under the same conditions (Scheme 1). The overall yields for both Ir(III) dipyrrinato and Ir(III) acetylacetonato complexes are in the range of 56–67%, which means that these functional Ir(III) phosphors can be readily prepared using this synthetic method. All of the Ir(III) phosphors are air stable and characterized by the NMR spectroscopy and the matrix-assisted laser desorption ionization time of flight mass spectrometry (MALDI-TOF-MS). The proton, carbon and fluorine signals from the ^1H, ^{13}C and ^{19}F-NMR spectra and the exact values of molecular mass confirm the identity of the target Ir(III) complexes (see Figures S1–S18 in the ESI).

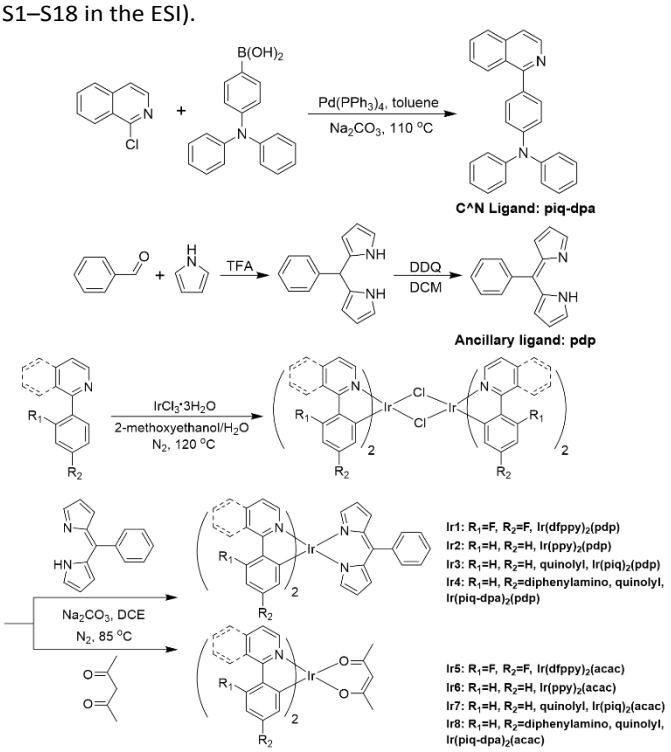

Scheme 1. Synthetic schemes for the preparation of ligands and Ir(III) phosphors **Ir1**-**Ir8**.

Single-crystal X-ray crystallography

The single crystals of **Ir2**, **Ir3** and **Ir7** were successfully obtained through the slow diffusion of hexane or methanol into their solutions in chloroform or dichloroethane. Their structures were determined by the single-crystal X-ray crystallography (Figure 1), in which six-coordinated geometries are observed. Moreover, the single crystal data of **Ir6** was accessible from the Cambridge Structural Database (CSD) of Cambridge Crystallographic Data Centre (CCDC). Their selected bond lengths and angles around the iridium center are summarized (Table S1, ESI). The X-ray data of **Ir2**, **Ir3** and **Ir7** reveal that the complexes adopt a monoclinic crystal system (Table 1). The bond lengths between the iridium center and the *pyrrolyl*-N, *pyridyl*-N and carbon atoms in **Ir2** and **Ir3** are almost constant, respectively, at ~2.13, ~2.05 and ~2.02 Å. In addition, the bond angles formed between the two *pyridyl*-N and iridium atoms in **Ir2** and **Ir3** are respectively 173.2° and 171.2°, while the bond angles formed between the two *pyrroly*-N and iridium atoms in **Ir2** and **Ir3** are 86.6° and 87.2°, respectively. By comparison, the bond angles formed by the two *pyridyl*-N and Ir atoms in **Ir6** and **Ir7** are 176.3° and 173.97°, while the bond angles formed by the two O and Ir atoms in **Ir6** and **Ir7** are 90.0° and 86.76°. These values are similar to the corresponding angles in the dipyrrinato complexes. Furthermore, the C^N ligands in **Ir2** and **Ir3** deviate from planarity around the bridging $C_{pyridyl}$–C_{phenyl} bond with the dihedral angles of 5.35° and 19.22°, respectively. Concurrently for **Ir6** and **Ir7**, the corresponding angles are 4.94° and 10.12°, respectively, indicating that the quinolyl moiety could generate a larger steric hindrance than the pyridyl moiety and the **pdp** ligand would produce a larger dihedral angle than that for the **acac** ligand. Moreover, the coordinated dipyrrinato ligand is also tilted away from a plane formed by the iridium center and the two pyrrolyl-N atoms, where the tilt angles between the dipyrrinato ligand and the coordination plane for **Ir2** and **Ir3** are 12.96° and 0.52°, respectively. The dihedral angles between the dipyrrin and phenyl moiety in the dipyrrinato residue for **Ir2** and **Ir3** are 66.46° and 71.13°, respectively. In addition to the packing mode in two crystals, steric hindrance and electronic effect of quinolyl group are responsible for these differences.

Table 1. Single crystal data parameters for structures **Ir2**, **Ir3**, **Ir6** and **Ir7**.

	Ir2[a]	**Ir3**[a]	**Ir6**[b]	**Ir7**[a]
Formula	$C_{37}H_{27}IrN_4$	$C_{45}H_{31}IrN_4$	$C_{27}H_{23}IrN_2O_2$	$C_{35}H_{27}IrN_2O_2$
Formula weight	719.82	819.94	599.67	699.78
Temperature/K	100(10)	100(10)	173(2)	293(2)
Crystal system	monoclinic	monoclinic	orthorhombic	monoclinic
Space group	$P2_1/c$	$C2/c$	$Pbcn$	$P2_1/c$
a/Å	18.7181(15)	14.9080(8)	13.171(3)	10.6958(6)
b/Å	9.2996(5)	25.4347(14)	10.086(2)	18.4049(12)
c/Å	17.7227(16)	10.7746(6)	16.613(3)	14.5378(9)
α/°	90.00	90.00	90.00	90.00
β/°	111.834(10)	107.152(5)	90.00	106.254(6)
γ/°	90.00	90.00	90.00	90.00
Volume/Å^3	2863.7(4)	3903.8(4)	2206.9(8)	2747.5(3)
Z	4	4	4	4
ρ_{calc}/g cm^{-3}	1.670	1.395	1.805	1.692
μ/mm^{-1}	4.696	3.455	6.077	4.895
F(000)	1416.0	1624.0	1168.0	1376.0
Crystal size/mm^3	0.11×0.1×0.08	0.13×0.12×0.1	N/A	0.13×0.11×0.1
ϑ range (deg)	4.62–50.00	4.44–50.00	4.90–45.00	3.97–50.00
No. of diffrn rflns	13690	8694	1410	12179
Total no. of rflns	5034	3444	2176	4829
No. of params	379	228	71	367
GOF on F^2	1.114	1.022	N/A	1.049
Final R indexes [$I \geq 2\sigma(I)$]	R_1 =0.0581, wR_2 = 0.1276	R_1 =0.0438, wR_2 = 0.0875	R_1 = N/A, wR_2 = N/A	R_1 =0.0374, wR_2 = 0.0757
Final R indexes [all data]	R_1 =0.0758, wR_2 = 0.1371	R_1 =0.0547, wR_2 = 0.0927	R_1 =0.0870, wR_2 = N/A	R_1 =0.0517, wR_2 = 0.0830

[a]The crystals were obtained through the slow diffusion of hexane or methanol into the chloroform or dichloroethane solutions of Ir(III) complexes. [b]The crystal data are accessible from the Cambridge Structural Database (CSD) of Cambridge Crystallographic Data Centre (CCDC).

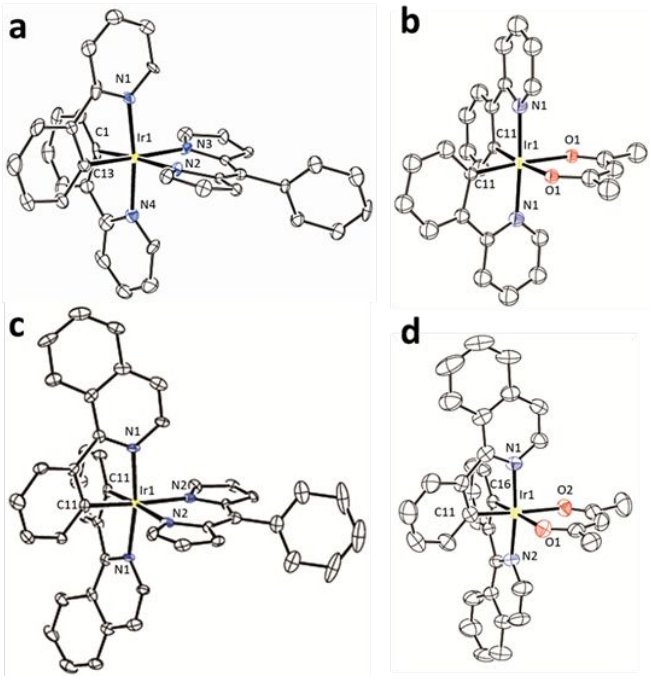

Figure 1. The crystal structures of (a) **Ir2**, (b) **Ir6**, (c) **Ir3**, (d) **Ir7**.

Thermal and photophysical properties

The thermal properties of **Ir1-Ir4** have been tested by thermogravimetric analysis (TGA) under a nitrogen flow (Figure S19, ESI). The TGA results provide information on the

thermal stability. For these complexes, the decomposition temperatures (T_d) are over 300 °C (the onset decomposition temperature at 5% degradation). The introduction of the quinolyl group increases the T_d presumably due to its rigid structural feature. Such good thermal properties of these synthetic phosphors proved that they can be sublimed by using the thermal vacuum deposition for the fabrication of OLED devices.

The absorption spectra of **Ir1**-**Ir8** in dichloromethane at 298 K are presented in Figure 2. All complexes show high-energy absorption bands at around 250 nm with larger molar extinction coefficients, which can be assigned to the ligand centered (LC) π–π* allowed transition of the cyclometalated C^N ligands. In particular, the LC transitions of **Ir3**-**Ir4** and **Ir7**-**Ir8** are extended to 300 nm due to the larger degree of π conjugation in the structures. The weaker absorption bands located between 320 and 450 nm are ascribed to the metal-to-ligand charge-transfer (MLCT) transitions. Similarly, the MLCT transitions of **Ir3**-**Ir4** and **Ir7**-**Ir8** are extended to 500 nm. For **Ir4** and **Ir8** that contain the diphenylamino group, both complexes exhibit an obvious intramolecular charge transfer (ICT) absorption band at around 400 nm, which should be mainly induced by the CT process arising from the non-bonding orbital n(N) to π* orbital of aryl group. All four Ir(III) dipyrrinato complexes exhibit an intense absorption band assigned to the ligand-centered (LC) π–π* transition of the 5-phenyldipyrrin ligand at around 480 nm, while the ancillary ligand of four Ir(III) acetylacetonato complexes does not exhibit this homologous transition in the visible absorption range.

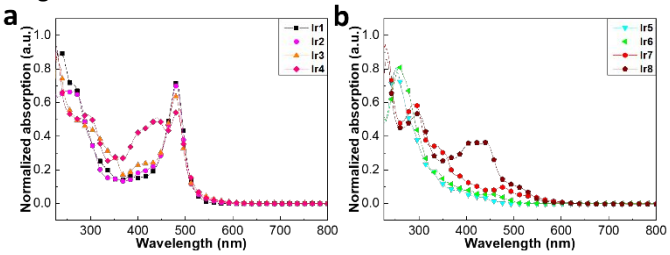

Figure 2. UV–vis absorption spectra of the Ir(III) complexes **Ir1**-**Ir4** (left) and **Ir5**-**Ir8** (right) in CH_2Cl_2 solution at 298 K.

The excitation spectra (at the monitoring wavelength of 685 nm) of all four Ir(III) dipyrrinato complexes in CH_2Cl_2 solution at 298 K have been measured and exhibit similar spectral lines to each other, notably for the band located at 550 nm, which corresponds to the LC transition of the dipyrrinato ligand. Upon excitation at 550 nm, all four Ir(III) complexes in CH_2Cl_2 solution at room temperature exhibit an emission band extending to the NIR region with a maximum at around 685 nm and a shoulder at around 740 nm (Figure 3a). Remarkably, the resulting phosphorescence bands of **Ir1**-**Ir4** do not show a bathochromic shift. It can conclude that the substituted decoration of C^N ligands does not influence the emission bands regardless of whether an electron-withdrawing group (fluorine), electron-donating group (diphenylamino) or extended conjugated group (quinolyl) is introduced. For comparison, the four corresponding Ir(III) acetylacetonato complexes were also examined and their emission spectra in CH_2Cl_2 at 298 K exhibit the expected bathochromic shift of their emission bands. As the introduction of fluorine (F) on the phenyl moiety can dramatically increase the electron deficiency at the *meta*-position ($C_{C\text{-}Ir}$), the *σ*-donation from C^N dfppy ligand to the d orbitals of Ir(III) center decreases and the ^{3}MLCT energy level is destabilized, leading to the blue-shifted emission of **Ir5** by about 30 nm compared to that of **Ir6**. By replacing the pyridyl moiety with a quinolyl moiety, the luminescence band of **Ir7** is red-shifted by ca. 100 nm to ca. 625 nm because the extended conjugation of cyclometalated ligands lowers the LUMO level of this Ir(III) complex. With the additional introduction of an electron-donating diphenylamino group onto the **piq** ligand, the energy of the HOMO level of the complex is raised so that **Ir8** emits at 645 nm representing a larger red-shift by 20 nm in comparison with that of **Ir7**. The emission quantum yields (Φ_{em}) of Ir(III) dipyrrinato complexes in degassed toluene solution were measured with **Ir2** as a standard (0.06).[39] The Φ_{em} of **Ir1**, **Ir3** and **Ir4** are in the range of 0.02-0.06. The relatively low Φ_{em} may stem from two reasons: 1) rotation motions of the phenyl ring and 2) large mass of the dipyrrinato ligand. Besides, while there is the intrinsic "energy gap law" notable in the NIR region, the coupling between the zero vibrational level of the S_1 (or T_1) state and the higher vibrational levels of the S_0 state can induce an enhanced nonradiative process.[40] On the other hand, the τ_{em} values of **Ir1**-**Ir4** were measured in doped films (10 wt% phosphors in CBP) at room temperature, and are 12.97, 2.76, 2.92 and 2.57 μs, respectively (Table 2).

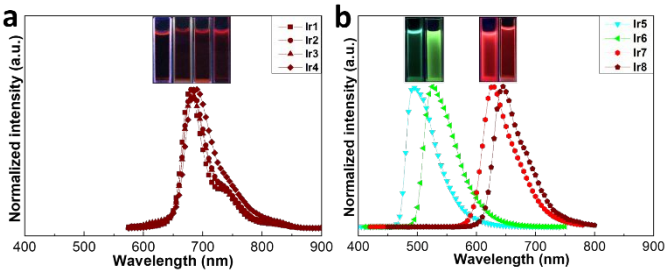

Figure 3. Photoluminescence spectra of the Ir(III) complexes **Ir1**-**Ir4** (left) and **Ir5**-**Ir8** (right) in CH_2Cl_2 solution recorded at 298 K, insets are the corresponding emission colors of Ir(III) complexes in CH_2Cl_2 solutions.

Table 2. Photophysical data and frontier orbital energy levels of the four Ir(III) dipyrrinato complexes.

Complex	$\lambda_{abs,max}$[a] (nm)	$\lambda_{PL,max}$[a] (nm)	Φ_{em}[b]	τ_{em}[c] (μs)	HOMO [eV]	LUMO [eV]
Ir1	385, 481	679	0.02	12.97	-5.38[d], -5.40[e]	-2.87[d], -2.15[e]
Ir2	407, 481	682	0.06	2.76	-5.28[d], -5.28[e]	-2.84[d], -2.06[e]
Ir3	425, 480	683	0.06	2.92	-5.24[d], -5.26[e]	-2.83[d], -2.07[e]
Ir4	441, 482	687	0.05	2.57	-5.05[d], -4.93[e]	-2.82[d], -2.05[e]

[a]Measured in CH_2Cl_2 at room temperature. [b]Calculated by referencing the integrated emission intensity to that of **Ir2** (Φ_{em} = 0.06). [c]Measured in films

(10 wt% phosphors in CBP) at room temperature. [d]Energy levels estimated from CV curves. [e]Energy levels estimated from the DFT calculation results.

Theoretical computations

Density functional theory (DFT) and time-dependent density functional theory (TD-DFT) calculations were used to rationalize the spectral properties and electronic structures of the **Ir1**-**Ir8** complexes. All the data are placed in Figures S20-S61 and Tables S2-S27. The computed bond lengths and angles after geometry optimization compare favourably to the X-ray data in general (Figure S20, ESI). However, calculated Ir-*pyridyl*-N distances tend to be slightly overshoot by approximately 0.03 Å in **Ir1**-**Ir4** and 0.04 Å in **Ir5**-**Ir8** on average. The same trends were observed for Ir-*pyrroly*-N and Ir-O_1 distances with a difference of about 0.05 Å. Additionally, some of the computed angles deviate up to nearly 3° in **Ir3** for *pyridyl*-N-Ir-*pyridyl*-N angle. The Root-Mean-Square Deviation (RMSD) of atomic positions were calculated for **Ir2**, **Ir3**, **Ir6** and **Ir7** and are included between 3.60 and 6.26 Å. The discrepancies between an optimized geometry and a structure in the crystalline phase may arise mainly from the difference in the environment of the Ir(III) complexes (*i.e.*, isolated *versus* packed). The optimization processes were performed using a CH_2Cl_2 solvent field, while in the crystal structure the complexes show constraint from the packing.

After geometry optimisation in both the ground and lowest energy triplet states, their total energies ($E(S_0)$ and $E(T_1)$; Figures S24, S29, S34, S39, S44, S49, S54 and S59)) are used to estimate the position of the triplet emissions ($E(T_1) - E(S_0) = D$ in eV, converted in nm). The calculated positions (*i.e.*, 0-0) are as follows (in increasing order): 415 (**Ir5**) < 449 (**Ir6**) << 532 (**Ir7**) < 577 (**Ir8**) << 656 (**Ir1**) = 656 (**Ir2**) ~ 653 (**Ir3**) = 656 (**Ir4**). This order follows the same trend observed with the experimental spectra of Figure 3. The experimental data are as follows (also in increasing order): 493 (**Ir5**) < 525 (**Ir6**) << 628 (**Ir7**) < 645 (**Ir8**) < 679 (**Ir1**) ~ 682 (**Ir2**) ~ 683 (**Ir3**) ~ 687 (**Ir4**). The comparison between the experimental and calculated data first indicates that the computations undershoot by 65-93 nm for **Ir5**-**Ir8** and 23-31 nm for **Ir1**-**Ir4**. Second, this comparison is acceptable for the former series (**Ir5**-**Ir8**) and is actually very good for the second series (**Ir1**-**Ir4**). It is noteworthy that experience proves that a perfect match is rarely observed. Indeed, a number of issues may explain these differences such as the slight structural differences between the X-ray data and those from the optimized geometry in the gas phase, the use of the emission maxima as the peak position, which is not necessarily the true 0-0 peak (the emission spectral envelope is a little broad), and the slight occasional difficulty of Gaussian to describe charge transfer character of molecules and complexes. Altogether, these issues can induce these differences. The fact that the trends are identical indicates that the conclusions drawn below are reliable. Similarly, the position of the first 100 spin-allowed transitions were computed allowing for the calculations of simulated absorption spectra (Figures S25, S30, S35, S40, S45, S50, S55 and S60) and extracting the lowest energy spin-allowed transitions (*i.e.*, 0-0 peaks; Tables S4, S7, S10, S13, S16, S19, S22, S25). The comparison between the calculated and experimental values shows the differences ranging from 8 to 30 nm (Table 26), which is considered very good. The comparison of the simulated and experimental absorption spectra is reasonable when taking into account that the simulated spectra do not compute the vibrational progression (Figure S61).

In addition to these computational investigations, the atomic contributions for both the frontier MOs have been calculated, thus permitting us to probe the nature of the singlet and triplet excited states. The MO representations (Figures S22, S24, S27, S32, S34, S37, S39, S42, S44, S47, S52, S54, S57, S59) and computed atomic contributions of the HOMO-4 to LUMO+4, LOSOMO and HSOMO (Tables S2, S3, S5, S6, S8, S9, S11, S12, S14, S15, S17, S18, S20, S21, S23, S24) of complexes **Ir1**-**Ir8** are presented in **Figure 4a, b** and in the ESI. The resemblance of the LUMO with HSOMO (high-lying semi-occupied MO) is striking. Moreover, two distinct families are depicted: **Ir1**-**Ir4**, and **Ir5**-**Ir8**. Based on the changes in atomic contributions upon comparing the HOMO with the LUMO (and the LSOMO with the HSOMO), assignments for the low-energy excited states have been proposed and are 1) a mixture of intraligand ππ* (L = dfppy, ppy, piq, piq-dpa) and MLCT for the series **Ir5**-**Ir8** (the contribution of the acac ligand is minor), 2) M/LL'CT (M = Ir, L = ppy, piq, piq-dpa, L' = pdp) for **Ir2**-**Ir4**, and 3) intraligand ππ* (L = pdp) for **Ir1**.

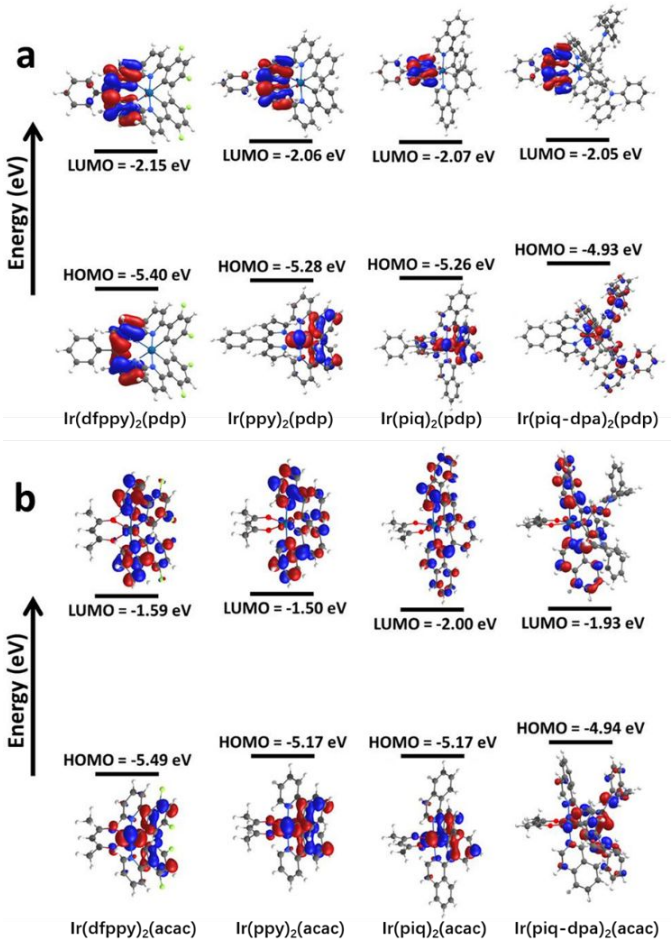

Figure 4. Representations of the HOMO and LUMO energy levels for the optimized geometry of **Ir1**-**Ir8**.

Electrochemical properties

The cyclic voltammetry (CV) had been performed without and with ferrocene used as an internal standard under N_2 to investigate the electrochemical properties of the eight Ir(III) phosphors (Figure 6). In the cathodic scan, the four Ir(III) dipyrrinato complexes **Ir1**-**Ir4** exhibit a reversible reduction wave with potential (E_{re}) at ca. -1.48 V, which can be assigned to the reduction of the pyrrolyl unit in the 5-phenyldipyrrin ligand. It is worth noting that the F atom in C^N ligands of **Ir1** can furnish a slightly lower reduction potential of the pyrrolyl moiety, presumably because F can induce an electron deficiency at the *meta*-position ($C_{C\text{-}Ir}$). Thus, the σ-donation from dipyrrinato ligand to the d orbitals of Ir(III) center increases and the pyrrole rings become easier to reduce. Conversely, the electron-donating diphenylamino substituent in **Ir4** could induce the reduction potential to be slightly higher up to ca. -1.50 V, showing that the pyrrole rings are more reluctant to be reduced. In the meantime, the four acetylacetonate-containing Ir(III) complexes, **Ir5**-**Ir8**, exhibit no reduction wave in the similar potential range, indicating that the ancillary ligand **acac** plays a very minor role on defining the nature of the LUMO manifold.

Multiple oxidation processes have also been observed for these heteroleptic Ir(III) complexes. All eight Ir(III) phosphors present the oxidation waves in the anodic sweep, which can be ascribed to the oxidation of the Ir center. **Ir1** exhibits the highest oxidation potential at 1.06 V in the four Ir(III) dipyrrinates, testifying that the fluorination can obviously lower the electron density on the Ir center. **Ir4** has the lowest oxidation potential at 0.73 V since the electron-donating group NPh_2 could provide electron density to the Ir center. For the same reason, **Ir5** exhibits the highest oxidation potential at 1.14 V in the four Ir(III) acetylacetonates with the introduction of a F atom. Concurrently, the lowest oxidation potential (at 0.70 V) is observed for **Ir8** due to the influence of the electron-donating diphenylamino moiety. The E_{ox}/E_{red} values as determined by CV are listed in Table S27, and the corresponding HOMO and LUMO energy levels for the eight Ir(III) complexes **Ir1**-**Ir8** can be calculated with reference to ferrocene.

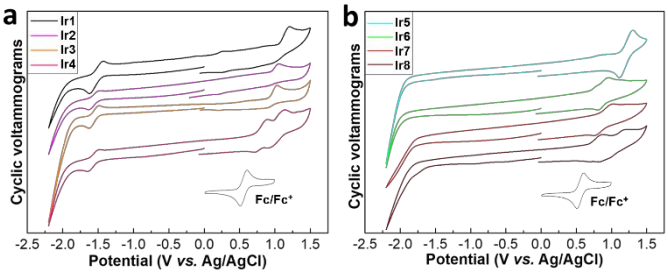

Figure 5. Cyclic voltammograms (CV) of the Ir(III) complexes **Ir1**-**Ir4** (left) and **Ir5**-**Ir8** (right) in CH_2Cl_2 solution (ferrocene is used as an internal standard).

Electroluminescent OLED performance

The electroluminescent (EL) spectra of the four Ir(III) dipyrrinato complexes were evaluated upon the fabrication of the OLED devices where these phosphors were used as dopants in the emissive layer (EML). We chose the thermal vacuum deposition to fabricate the OLEDs due to their good thermal stabilities. The device structures are: ITO/HATCN (20 nm)/TAPC (40 nm)/mCP (5 nm)/Ir (x wt%): CBP (30 nm)/TPBi (40 nm)/LiF (1 nm)/Al (100 nm) (Figure 7). In the configuration of OLEDs, the hole flows from indium tin oxide (ITO), while dipyrazino [2,3-*f*:2′,3′-*h*]quinoxaline-2,3,6,7,10,11-hexacarbonitrile (HATCN) is utilized as the hole injection layer, 4,4′-(cyclohexane-1,1-diyl)bis(*N*,*N*-di-*p*-tolylaniline) (TAPC) and 1,3-di(9*H*-carbazol-9-yl) benzene (mCP) are both used as the hole transport layers, in which 5 nm mCP also plays the role of electron-blocking, the well-known 4,4′-N,N′-dicarbazole-biphenyl (CBP) is the host material in which the phosphorescent Ir complexes are used as dopant, while 1,3,5-tris[N-(phenyl)-benzimidazole]benzene (TPBi) serves as the functional layer for both electron-transporting and hole-blocking, LiF is utilized as the electron injection layer, and the electron flows from Al. Besides, the variation of the doping levels for **Ir3** has been carried out for the purpose of optimizing the EL performance of OLEDs.

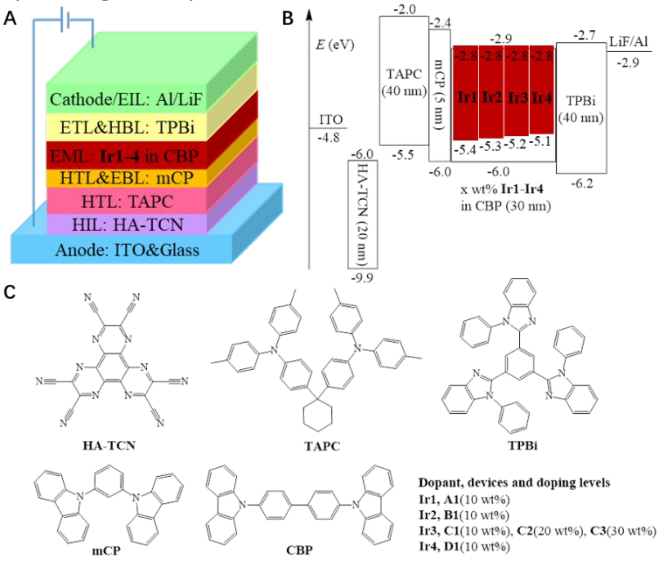

Figure 6. Device structure, energy level diagram and molecular structures of the materials for the OLEDs.

When a proper voltage was applied, all OLED devices displayed the deep red (DR) to NIR electroluminescence. The maxima of the EL peaks are consistent with the PL spectra of the corresponding Ir(III) phosphors, indicating that the EL emissions indeed result from the triplet excited states of the metallophosphors. In addition, no emission from CBP was detected in the devices, suggesting the efficient energy transfer from the host excitons to the metallophosphor dopants and the inner confinement of the metallophosphor excitons. The OLED devices exhibited turn-on voltages (at a luminance of 1 cd/cm^2) in the range of 5.0 to 7.5 V. The J–V–L characteristics and EL efficiency-current density curves for the OLEDs are shown in Figure 8. The detailed EL results are listed

in Table 3. The device **C1** based on **Ir3** at a doping level of 10 wt% showed the highest EL efficiency among all these DR-NIR emitting devices with a EQE of 2.8%. The EQEs afforded by the DR-NIR OLED devices based on our designed Ir(III) dipyrrinato complexes are better than many DR-NIR OLEDs based on the Ir(III) complexes employing the cyclometalated ligands with extended conjugations,[41-43] but are still not yet competitive to the devices based on the current state-of-the-art Ir(III) emitters.[19, 44-45] Changing the structures of the cyclometalated C^N ligands has a minimal effect on the OLED performance. The maximum EQE for device **A1** based on **Ir1**, device **B1** based on **Ir2** and device **D1** based on **Ir4** are 2.7%, 2.1% and 2.5%, respectively. All the devices showed a relatively low current efficiency (CE) and power efficiency (PE) that may be ascribed to the relatively low luminous intensity and luminous flux in the DR-NIR region. Moreover, it is found that the increase of doping levels (*i.e.*, 10%, 20% and 30% of **Ir3**) caused a minimal decrease in EQE, CE and PE of OLEDs (Figure S62 and Table S28, ESI). For other applications, these NIR emitting Ir(III) dipyrrinato complexes are also expected to exhibit the potential advantages in the biotechnological field.[46]

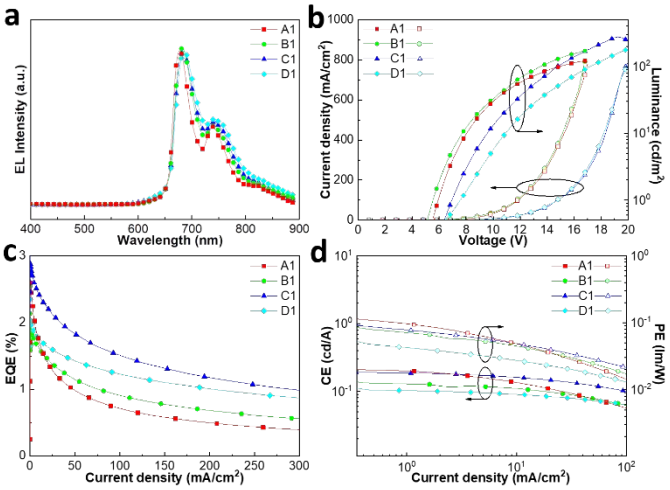

Figure 7. (a) Electroluminescence spectra, (b) current density-voltage-luminance (*J*-*V*-*L*) curves, (c) EQE-current density curves, (d) curves of CE and PE versus current density for devices **A1**-**D1**.

Table 3. The EL performance of OLEDs **A1**-**D1**.

Device	EQE [%]	L_{max} [cd m^{-2}]	λ_{max}[nm]	V_{on} [V][c]	CIE [x, y]
A1	2.7[a], 0.7[b]	120	678, 739	5.5	0.69, 0.29
B1	2.1[a], 0.9[b]	170	682, 741	5.9	0.67, 0.29
C1	2.8[a], 1.5[b]	280	684, 743	6.9	0.70, 0.29
D1	2.5[a], 1.2[b]	190	685, 744	7.5	0.70, 0.28

[a]Maximum efficiency. [b]Efficiency recorded at the current density of 100 mA cm^{-2}. [c]Turn-on voltage recorded at the luminance of 1 cd m^{-2}.

Experimental section

All commercially available starting materials were used directly with no further purification. **Ir6** and **Ir7** were purchased from Aldrich or TCI and used without further purification. The solvents were dried prior to use. All the reactions were carried out under an atmosphere of N_2 using standard Schlenk techniques and were monitored by thin-layer chromatography (TLC) with Merck pre-coated glass plates. Flash column chromatography was performed using the silica gel purchased from Qingdao Haiyang Co., Ltd. Purification of the products was achieved *via* silica column chromatography with hexane/ dichloromethane or hexane/ethyl acetate mixed solvents as eluents. Compounds were visualized under UV light irradiation at 254 or 365 nm. ^{1}H NMR, ^{13}C NMR and ^{19}F NMR spectra were recorded in $CDCl_3$ solvent on a Bruker Avance 400 MHz spectrometer, which were calibrated using residual non-deuterated solvent peaks as an internal reference. The chemical shifts (δ) are reported in ppm and the coupling constants (J) are expressed in Hertz (Hz). Mass spectra were obtained on a Bruker Autoflex matrix assisted laser desorption ionization time-of-flight mass spectrometer (MALDI-TOF MS). Thermal gravimetric analysis (TGA) data were collected on a Perkin-Elmer TGA thermal analyzer under a N_2 atmosphere with a heating rate of 10 °C/min. The UV-vis absorption spectra of synthetic Ir(III) complexes were measured on Cary UV-300 spectrophotometer at room temperature using the quartz cuvette as the holder. Perkin-Elmer LS 55 fluorescence spectrometer was used to detect the photoluminescent spectra. All eight Ir(III) complexes were subjected to the electrochemical tests for cyclic voltammetry on CH Instruments CHI800D Serials electrochemical analyzer with the scan rate of 0.1 V/s via a set-up of three electrode system (working electrode: glassy carbon disk, reference electrode: Ag/AgCl immersed in saturated potassium chloride solution before use, counter electrode: Pt wire). The redox couple of ferrocene/ferrocenium (Fc/Fc^+) was used as the internal standard. The electrolyte was a dichloromethane solution of 0.1 M $[Bu_4N]PF_6$ and was degassed with nitrogen, and all CV measurements were performed under a N_2 atmosphere.

X-ray crystallography

Crystal data of **Ir2**, **Ir3** were collected at 100 K and **Ir7** at 293 K on a Rigaku Oxford Diffraction Supernova Dual Source equipped with an AtlasS2 CCD using Cu Kα radiation. Data reduction was carried out with the diffractometer's software (Agilent Technologies, CrysAlisPRO, Version 2013). The structures were solved by direct methods using Olex2 software, and the non-hydrogen atoms were located from the trial structure and refined anisotropically with SHELXL-2018 using a full-matrix least squares procedure based on F^2. The weighted R factor, wR_2 and goodness-of-fit S values were obtained based on F^2. The hydrogen atom positions were fixed geometrically at the calculated distances and allowed to ride on their parent atoms. Crystallographic data for the structure reported in this paper have been deposited at the Cambridge Crystallographic Data Center and allocated with the deposition numbers: CCDC 2005395, 2005396 and 2005397 for compounds **Ir2**, **Ir3** and **Ir7** respectively.

Computational details

All density functional theory (DFT) and time dependent (TD-DFT) calculations were performed with Gaussian 16[47] at the Université de Sherbrooke with the Mammouth supercomputer supported by *Le Réseau Québécois De Calculs Hautes Performances*. DFT (ground and triplet state optimisations) and TD-DFT[48-57] calculations were carried out using the B3LYP/genecp method. A 6-31g (d, p) basis set was used for C, H, N, O and F atoms.[56] VDZ (valence double ζ) with SBKJC effective core potentials was used for Ir atoms.[58-63] A dichloromethane (CH_2Cl_2) solvent field (cpcm) was applied to all calculations. Red color corresponds to the positive isosurface, while the blue one corresponds to the negative isosurface. The calculated electronic absorption spectra were obtained using GaussSum 3.0.[64] No imaginary frequencies were observed, confirming the correct energy minimization during optimization process.

OLED fabrication and measurements

The device layers of HAT-CN (20 nm)/TAPC (40 nm)/mCP (5 nm)/phosphor doped in CBP (10 wt%, 30 nm)/TPBi (40 nm)/LiF (1 nm)/Al (100 nm) were successively deposited on the pre-cleaned ITO glass substrates with the thermal evaporation rate of 0.5~1 Å/s at a pressure of less than 10^{-6} Torr. For each device, four pixels with the same device configuration were prepared at one batch, and the deposited Al cathode overlaps with the precoated ITO anode to fabricate an active area of 2 mm × 2 mm for each pixel. The EL spectra of devices were measured by the fiber optic spectrometer (Ocean Optics USB 2000) in the normal direction. The current density-voltage-luminance (J-V-L) curves were investigated by a dual-channel Keithley 2614B source measure unit and a PIN-25D silicon photodiode.

General procedure for the synthesis of the ligands

For cyclometalated C^N ligand **piq-dpa**, 4-(diphenylamino)phenylboronic acid (1.0 equiv) and 1-chloroisoquinoline (1.1 equiv) were added into a toluene, EtOH and H_2O mixed solvents (7:1:2, v/v/v) under a N_2 atmosphere. $Pd(PPh_3)_4$ (0.05 equiv) and K_2CO_3 (1.0 equiv) were added into the reacting system. The reaction was allowed to proceed at 110 °C for 18 h. After cooling to room temperature, the mixture was diluted by adding 100 mL of ethyl acetate and washed with water. The collected organic solvent was removed under reduced pressure. The residue was purified by silica gel column chromatography eluting with hexane/CH_2Cl_2 to give a pale gray compound (Scheme 2).

For ancillary ligand 5-phenyldipyrrin, benzaldehyde (1.0 equiv) was added in excessive pyrrole and TFA (5.0 equiv) was added with stirring for 2 h at room temperature under N_2. The unreacted pyrrole was removed under reduced pressure. The crude product was purified by silica column chromatography to afford 5-phenyldipyrromethane. Then, the intermediate product was allowed to react with the oxidizing agent DDQ (1.5 equiv) to give the dipyrrinato ligand, 5-phenyldipyrrin. Without further purification the activated ligand was directly used to react with Ir(III) μ-chlorobridged dimers. Other ligands were purchased from Aldrich or TCI, and used without further purification (Scheme 3).

Piq-dpa (yield, 76%). ^{1}H NMR (400 MHz, $CDCl_3$) δ 8.59 (d, J = 5.7 Hz, 1H), 8.23 (dd, J = 8.5, 1.0 Hz, 1H), 7.91 – 7.86 (m, 1H), 7.70 (d, J = 1.3 Hz, 1H), 7.65 – 7.52 (m, 4H), 7.35 – 7.27 (m, 4H), 7.23 (d, J = 2.1 Hz, 1H), 7.22 – 7.18 (m, 5H), 7.08 – 7.04 (m, 2H). ^{13}C NMR (101 MHz, $CDCl_3$) δ 160.44, 148.49, 147.66, 142.30, 137.10, 131.07, 130.11, 129.45, 129.16, 127.80, 127.21, 127.13, 126.76, 124.88, 123.34, 123.07, 122.93, 119.69. MS (MALDI-TOF) [m/z]: found $[M]^+$ 373.1710, calculated 373.1699 ($C_{27}H_{20}N_2$).

5-Phenyldipyrromethane (yield, 60%). ^{1}H NMR (400 MHz, $CDCl_3$) δ 7.93 (s, 2H), 7.39 – 7.31 (m, 2H), 7.31 – 7.27 (m, 1H), 7.26 – 7.20 (m, 2H), 6.71 (td, J = 2.6, 1.5 Hz, 2H), 6.19 (dt, J = 3.4, 2.7 Hz, 2H), 5.94 (dddd, J = 3.4, 2.5, 1.6, 0.9 Hz, 2H), 5.49 (s, 1H). ^{13}C NMR (101 MHz, $CDCl_3$) δ 142.18, 132.61, 128.77, 128.52, 127.10, 117.35, 108.54, 107.34, 44.09. MS (MALDI-TOF) [m/z]: found $[M-H]^+$ 221.2866, calculated 222.1157 ($C_{15}H_{14}N_2$).

General procedure for the synthesis of the iridium(III) complexes

Under a N_2 atmosphere, the corresponding C^N ligand (2.2 equiv) and $IrCl_3{\cdot}nH_2O$ (1.0 equiv, 60 wt % Ir content) were allowed to react in a mixture of 2-methoxyethanol and water (3:1, v/v) at 110 °C for 24 h. The reaction mixture was cooled to room temperature and deionized water was added to precipitate the cyclometalated Ir(III) μ-chlorobridged dimer. The solids were filtered, collected and dried under vacuum. To synthesize Ir(III) dipyrrinato complex, the Ir(III) μ-chloro-bridged dimer, 5-phenyldipyrrin (3.0 equiv) and Na_2CO_3 (10.0 equiv) were added to dichloroethane and the mixture was heated to 85 °C for 12 h. By contrast, to synthesize Ir(III) acetylacetonates, the Ir(III) μ-chloro-bridged dimer, acetylacetone (5.0 equiv) and Na_2CO_3 (10.0 equiv) were added to dichloroethane and the mixture was heated to 85 °C for 12 h. After cooling to room temperature, both mixtures were washed with deionized water and the organic layers were removed under reduced pressure. The crude products were purified on a silica gel column using hexane/ethyl acetate (EA) or hexane/CH_2Cl_2 as eluent to get the corresponding pure samples (Scheme 4).

Ir1 (red, yield: 56%). ^{1}H NMR (400 MHz, $CDCl_3$) δ 8.24 (d, J = 8.4 Hz, 2H), 7.81 (d, J = 5.8 Hz, 2H), 7.68 (t, J = 7.8 Hz, 2H), 7.55 – 7.32 (m, 5H), 6.96 (t, J = 6.0 Hz, 2H), 6.78 (s, 2H), 6.51 (dd, J = 4.3, 1.2 Hz, 2H), 6.49 – 6.37 (m, 2H), 6.25 (dd, J = 4.3, 1.3 Hz, 2H), 5.78 (dd, J = 8.6, 2.4 Hz, 2H). ^{13}C NMR (101 MHz, CDCl3) δ 152.15, 149.74, 148.77, 139.40, 137.23, 134.28, 131.79, 130.46, 128.24, 127.17, 123.08, 122.88, 122.25, 117.44, 113.99, 97.47. ^{19}F NMR (377 MHz, $CDCl_3$) δ -108.51, -108.54, -110.67, -110.70. MS (MALDI-TOF) [m/z]: found $[M]^+$ 792.1494, calculated 792.1488 ($C_{37}H_{23}F_4N_4Ir$).

Ir2 (deep red, yield: 60%). ^{1}H NMR (400 MHz, $CDCl_3$) δ 7.89 – 7.84 (m, 2H), 7.82 (d, J = 7.9 Hz, 2H), 7.65 – 7.57 (m, 4H), 7.47 – 7.35 (m, 5H), 6.96 – 6.86 (m, 4H), 6.82 (td, J = 7.4, 1.3 Hz, 2H), 6.79 (t, J = 1.3 Hz, 2H), 6.48 (dd, J = 4.3, 1.3 Hz, 2H), 6.44 – 6.34 (m, 2H), 6.22 (dd, J = 4.3, 1.4 Hz, 2H). ^{13}C NMR (101 MHz, $CDCl_3$) δ 168.95, 156.76, 152.44, 149.74, 148.54, 144.69,

139.84, 136.13, 134.49, 132.35, 131.27, 130.52, 129.69, 127.98, 127.06, 123.97, 121.99, 120.86, 118.71, 117.10. MS (MALDI-TOF) [m/z]: found $[M]^+$ 720.1885, calculated 720.1865 ($C_{37}H_{27}N_4Ir$).

Ir3 (deep red, yield: 62%). ^1H NMR (400 MHz, $CDCl_3$) δ 8.95 (d, J = 9.3 Hz, 2H), 8.21 (d, J = 8.3 Hz, 2H), 7.85 (d, J = 6.4 Hz, 4H), 7.67 (d, J = 9.4 Hz, 4H), 7.49 – 7.35 (m, 5H), 7.24 (s, 2H), 6.99 (t, J = 7.2 Hz, 2H), 6.78 (t, J = 7.2 Hz, 2H), 6.64 (s, 2H), 6.49 (d, J = 4.1 Hz, 2H), 6.44 (d, J = 7.3 Hz, 2H), 6.19 (d, J = 4.1 Hz, 2H). ^{13}C NMR (101 MHz, $CDCl_3$) δ 169.73, 160.14, 152.35, 146.47, 142.19, 136.68, 134.53, 132.89, 131.33, 130.55, 130.01, 129.64, 127.96, 127.67, 127.25, 127.16, 127.05, 126.55, 120.58, 120.41, 117.18. MS (MALDI-TOF) [m/z]: found $[M]^+$ 820.2186, calculated 820.2178 ($C_{45}H_{31}N_4Ir$).

Ir4 (deep red, yield: 58%). ^1H NMR (400 MHz, $CDCl_3$) δ 8.82 – 8.69 (m, 2H), 8.01 (d, J = 8.8 Hz, 2H), 7.72 – 7.48 (m, 8H), 7.48 – 7.33 (m, 5H), 7.12 – 6.87 (m, 16H), 6.86 (t, J = 1.4 Hz, 2H), 6.80 (d, J = 6.5 Hz, 2H), 6.75 (tt, J = 7.0, 1.5 Hz, 4H), 6.69 (dd, J = 8.8, 2.5 Hz, 2H), 6.48 (dd, J = 4.3, 1.4 Hz, 2H), 6.27 (dd, J = 4.3, 1.4 Hz, 2H), 5.94 (d, J = 2.5 Hz, 2H). ^{13}C NMR (101 MHz, $CDCl_3$) δ 168.49, 161.54, 152.25, 148.31, 148.23, 147.03, 141.85, 139.99, 139.53, 136.43, 134.48, 131.14, 130.53, 130.39, 129.83, 128.79, 127.86, 127.16, 127.00, 126.96, 126.92, 125.96, 125.65, 124.16, 123.17, 118.87, 116.97, 113.42. MS (MALDI-TOF) [m/z]: found $[M]^+$ 1154.3639, calculated 1154.3648 ($C_{69}H_{49}N_6Ir$).

Ir5 (yellow, yield: 65%). ^1H NMR (400 MHz, $CDCl_3$) δ 8.44 (ddd, J = 5.8, 1.7, 0.8 Hz, 2H), 8.35 – 8.15 (m, 2H), 7.86 – 7.72 (m, 2H), 7.19 (ddd, J = 7.3, 5.8, 1.4 Hz, 2H), 6.33 (ddd, J = 12.6, 9.3, 2.4 Hz, 2H), 5.65 (dd, J = 8.8, 2.4 Hz, 2H), 5.26 (s, 1H), 1.81 (s, 6H). ^{13}C NMR (101 MHz, $CDCl_3$) δ 185.16, 165.49, 165.42, 164.12, 164.00, 162.30, 162.17, 161.59, 161.46, 159.73, 159.60, 151.41, 151.34, 148.19, 138.00, 128.80, 128.77, 128.73, 122.85, 122.66, 121.76, 115.32, 115.29, 115.15, 115.12, 100.85, 97.73, 97.46, 97.19, 28.81. ^{19}F NMR (377 MHz, $CDCl_3$) δ -108.82, -108.84, -111.07, -111.10. MS (MALDI-TOF) [m/z]: found $[M]^+$ 672.1058, calculated 672.1012 ($C_{27}H_{19}F_4N_2O_2Ir$).

Ir8 (red, yield: 67%). ^1H NMR (400 MHz, $CDCl_3$) δ 8.85 – 8.72 (m, 2H), 8.14 (d, J = 6.4 Hz, 2H), 7.98 (d, J = 8.9 Hz, 2H), 7.78 – 7.70 (m, 2H), 7.67 – 7.58 (m, 4H), 7.12 – 7.05 (m, 2H), 6.97 – 6.91 (m, 8H), 6.91 – 6.84 (m, 8H), 6.76 – 6.66 (m, 4H), 6.56 (dd, J = 8.8, 2.5 Hz, 2H), 5.83 (d, J = 2.5 Hz, 2H), 5.20 (s, 1H), 1.79 (s, 6H). ^{13}C NMR (101 MHz, $CDCl_3$) δ 184.66, 168.29, 152.47, 147.44, 146.90, 140.28, 139.22, 137.07, 130.25, 130.01, 128.71, 127.21, 126.99, 126.88, 125.95, 125.81, 124.48, 123.18, 118.24, 112.96, 100.76, 28.95. MS (MALDI-TOF) [m/z]: found $[M]^+$ 1034.3144, calculated 1034.3172 ($C_{59}H_{45}N_4O_2Ir$).

Conclusions

The electrochemical and photophysical properties of Ir(III) dipyrrinato complexes and Ir(III) acetylacetonato complexes were investigated and compared. Ir(III) acetylacetonates show the normal bathochromic effect while the Ir(III) dipyrrinates are reluctant to show bathochromic effect. This can be explained by the fact that the triplet energy levels of the ancillary ligand (**acac**) lie above those localized in the cyclometalated C^N ligand and MLCT excited states, but the dipyrrinato ligand (**pdp**) has the lowest triplet excited state. Thus, the C^N ligand dominates the emission of Ir(III) acetylacetonates. Conversely, the dipyrrinato ligand, and much less from the C^N ones, defines the nature of the emission of the Ir(III) dipyrrinates. This work should provide a different perspective on the control of the triplet excited states of Ir(III) complexes with the lower triplet-state energy of ancillary ligand which can change the optoelectronic properties of these organometallic complexes.

Conflicts of interest

There are no conflicts to declare.

Acknowledgements

W.Y.W. thanks the National Natural Science Foundation of China (51873176), Hong Kong Research Grants Council (PolyU153058/19P), Guangdong-Hong Kong-Macao Joint Laboratory of Optoelectronic and Magnetic Functional Materials (2019B121205002), Hong Kong Polytechnic University (1-ZE1C) and the Endowed Professorship in Energy from Ms Clarea Au (847S) for the financial support. P.D.H. thanks the Natural Sciences and Engineering Research Council of Canada (NSERC), the Fonds de Recherche du Québec-Nature et Technologies (FQRNT), Compute Canada and Calcul Québec, the Centre Quebecois sur les Matériaux Fonctionnels (CEMOPUS) for funding.

Notes and references

1 Y. Garcia, F. Robert, A. D. Naik, G. Zhou, B. Tinant, K. Robeyns, S. Michotte and L. Piraux, *J. Am. Chem. Soc.*, 2011, **133**, 15850-15853.
2 C. Grohmann, T. Hashimoto, R. Fröhlich, Y. Ohki, K. Tatsumi and F. Glorius, *Organometallics*, 2012, **31**, 8047-8050.
3 J. Chen, D. Unjaroen, S. Stepanovic, A. van Dam, M. Gruden and W. R. Browne, *Inorg. Chem.*, 2018, **57**, 4510-4515.
4 T. T. Meng, H. Wang, Z. B. Zheng and K. Z. Wang, *Inorg. Chem.*, 2017, **56**, 4775-4779.
5 A. Ito and Y. Matsui, *Inorg. Chem.*, 2019, **58**, 10436-10443.
6 J. L. Liao, Y. Chi, C. C. Yeh, H. C. Kao, C. H. Chang, M. A. Fox, P. J. Low and G. H. Lee, *J. Mater. Chem. C*, 2015, **3**, 4910-4920.
7 Y. Yuan, J. L. Liao, S. F. Ni, A. K. Y. Jen, C. S. Lee and Y. Chi, *Adv. Funct. Mater.*, 2020, **30**, 1906738.
8 A. K. Renfrew, N. S., Bryce and T. W. Hambley, *Chem. Sci.*, 2013, **4**, 3731-3739.
9 J. Wang, S. Chorazy, K. Nakabayashi, B. Sieklucka and S. I. Ohkoshi, *J. Mater. Chem. C*, 2018, **6**, 473-481.
10 T. Nishiura, A. Takabatake, M. Okutsu, J. Nakazawa and S. Hikichi, *Dalton Trans.*, 2019, **48**, 2564-2568.
11 C. Wang, L. A. Chen, H. Huo, X. Shen, K. Harms, L. Gong and E. Meggers, *Chem. Sci.*, 2015, **6**, 1094-1100.
12 F. Wei, S.-L. Lai, S. Zhao, M. Ng, M.-Y. Chan, V. W.-W. Yam, and K. M.-C. Wong, *J. Am. Chem. Soc*. 2019, **141**, 12863−12871.
13 M. A. Baldo, S. Lamansky, P. E. Burrows, M. E. Thompson and S. R. Forrest, *Appl. Phys. Lett.* 1999, **75**, 4–6.

14 S. Lamansky, P. Djurovich, D. Murphy, F. Abdel-Razzaq, H. E. Lee, C. Adachi, P. E. Burrows, S. R. Forrest and M. E. Thompson, *J. Am. Chem. Soc.*, 2001, **123**, 4304-4312.
15 J. B. Waern, C. Desmarets, L. M. Chamoreau, H. Amouri, A. Barbieri, C. Sabatini, B. Ventura and F. Barigelletti, *Inorg. Chem.*, 2008, **47**, 3340-3348.
16 X. Yang, G. Zhou and W. Y. Wong, *Chem. Soc. Rev.*, 2015, **44**, 8484-8575.
17 S. Lamansky, P. Djurovich, D. Murphy, F. Abdel-Razzaq, R. Kwong, I. Tsyba, M. Bortz, B. Mui, R. Bau and M. E. Thompson, *Inorg. Chem.*, 2001, **40**, 1704-1711.
18 J. Lee, H. F. Chen, T. Batagoda, C. Coburn, P. I. Djurovich, M. E. Thompson and S. R. Forrest, *Nat. Mater.*, 2016, **15**, 92-98.
19 Z. Chen, H. Zhang, D. Wen, W. Wu, Q. Zeng, S. Chen and W. Y. Wong, *Chem. Sci.*, 2020, **11**, 2342–2349.
20 E. Zysman-Colman (Editor), *John Wiley & Sons Ltd*, 2017, ISBN:9781119007166.
21 Y. You and S. Y. Park, *J. Am. Chem. Soc.*, 2005, **127**, 12438-12439.
22 T.-Y. Li, J. Wu, Z.-G. Wu, Y.-X. Zheng, J.-L. Zuo and Y. Pan, *Coord. Chem. Rev.*, 2018, **374**, 55-92.
23 G. Zhou, W. Y. Wong, B. Yao, Z. Xie and L. Wang, *Angew. Chem. Int. Ed.*, 2007, **46**, 1149-1151.
24 T. E. Wood and A. Thompson, *Chem. Rev.*, 2007, **107**, 1831-1861.
25 N. Boens, V. Leen and W. Dehaen, *Chem. Soc. Rev.*, 2013, **41**, 1130-1172.
26 S. Kusaka, R. Sakamoto, Y. Kitagawa, M. Okumura and H. Nishihara, *Chem. Asian J.*, 2012, **7**, 907-910.
27 V. S. Thoi, J. R. Stork, D. Magde and S. M. Cohen, *Inorg. Chem.*, 2006, **45**, 10688-10697.
28 S. Kusaka, R. Sakamoto and H. Nishihara, *Inorg. Chem.*, 2014, **53**, 3275-3277.
29 S. R. Halper and S. M. Cohen, *Inorg. Chem.*, 2005, **44**, 486-488.
30 R. K. Gupta, R. Pandey, R. Singh, N. Srivastava, B. Maiti, S. Saha, P. Li, Q. Xu and D. S. Pandey, *Inorg. Chem.*, 2012, **51**, 8916-8930.
31 C. Bronner, S. A. Baudron, M. W. Hosseini, C. A. Strassert, A. Guenet and L. De Cola, *Dalton Trans.*, 2010, **39**, 180-184.
32 G. Li, A. Yella, D. G. Brown, S. I. Gorelsky, M. K. Nazeeruddin, M. Grätzel, C. P. Berlinguette and M. Shatruk, *Inorg. Chem.*, 2014, **53**, 5417-5419.
33 T. M. McLean, J. L. Moody, M. R. Waterland and S. G. Telfer, *Inorg. Chem.*, 2012, **51**, 446-455.
34 X. Liu, H. Nan, W. Sun, Q. Zhang, M. Zhan, L. Zou, Z. Xie, X. Li, C. Lu and Y. Cheng, *Dalton Trans.*, 2012, **41**, 10199-10210.
35 C. Ikeda, S. Ueda and T. Nabeshima, *Chem. Commun.*, 2009, 2544-2546.
36 N. Sakamoto, C. Ikeda, M. Yamamura and T. Nabeshima, *J. Am. Chem. Soc.*, 2011, **133**, 4726-4729.
37 S. A. Baudron, *Dalton Trans.*, 2013, **42**, 7498-7509.
38 K. Hanson, A. Tamayo, V. V. Diev, M. T. Whited, P. I. Djurovich and M. E. Thompson, *Inorg. Chem.*, 2010, **49**, 6077-6084.
39 K. Takaki, E. Sakuda, A. Ito, S. Horiuchi, Y. Arikawa and K. Umakoshi, *Inorg. Chem.*, 2019, **58**, 14542-14550.
40 K. T. Ly, R.-W. Chen-Cheng, H.-W. Lin, Y.-J. Shiau, S.-H. Liu, P.-T. Chou, C.-S. Tsao, Y.-C. Huang and Y. Chi, *Nature. Photon.* 2017, **11**, 63–68.
41 Y. Liu, Z. R. Han, F. Y. Meng, P. Wang, L. Yang, Y. F. Wang, Y. Pei and S. J. Su, *Chem. Phys. Lett.,* 2018, **699**, 99–106.
42 G. Fu, H. Zheng, Y. He, W. Li, X. Lü and H. He, *J. Mater. Chem. C,* 2018, **6**, 10589–10596.
43 Z. R. Hao, M. Li, Y. J. Liu, Y. F. Wang, G. H. Xie and Y. Liu, *Dyes Pigm.,* 2018, **149**, 315–322.
44 C. You, D. Liu, M. Zhu, J. Yu, B. Zhang, Y. Liu, Y. Wang and W. Zhu, *J. Mater. Chem. C*, 2020, **8**, 7079–7088.
45 W. Li, B. Wang, T. Miao, J. Liu, G. Fu, X. Lü, W. Feng and W.-Y. Wong, *J. Mater. Chem. C,* 2021, **9**, 173–180.
46 L. Zhang, Y. Li, W. Che, D. Zhu, G. Li, Z. Xie, N. Song, S. Liu, B. Z. Tang, X. Liu, Z. Su and M. R. Bryce, *Adv. Sci.*, 2019, **6**, 1802050.
47 Gaussian 16, Revision B.01, M. J. Frisch, et al., Gaussian, Inc., Wallingford CT, 2016.
48 P. Hohenberg and W. Kohn, *Phys. Rev.*, 1964, **136**, B864–B871.
49 W. Kohn and L. J. Sham, *Phys. Rev.*, 1965, **140**, A1133–A1138.
50 R. G. Parr and W. Yang, *Density-functional theory of atoms and molecules*, Oxford University Press, 1989.
51 D. R. Salahub and M. C. Zerner (Eds), *The Challenge of d and f Electrons*, American Chemical Society, Washington, DC, 1989, vol. 394.
52 R. Bauernschmitt and R. Ahlrichs, *Chem. Phys. Lett.*, 1996, **256**, 454–464.
53 M. E. Casida, C. Jamorski, K. C. Casida and D. R. Salahub, *J. Chem. Phys.*, 1998, **108**, 4439–4449.
54 R. E. Stratmann, G. E. Scuseria and M. J. Frisch, *J. Chem. Phys.*, 1998, **109**, 8218–8224.
55 C. Lee, W. Yang and R. G. Parr, *Phys. Rev. B*, 1988, **37**, 785–789.
56 B. Miehlich, A. Savin, H. Stoll and H. Preuss, *Chem. Phys. Lett.*, 1989, **157**, 200–206.
57 A. D. Becke, *J. Chem. Phys.*, 1993, **98**, 5648–5652.
58 J. S. Binkley, J. A. Pople and W. J. Hehre, *J. Am. Chem. Soc.*, 1980, **102**, 939–947.
59 M. S. Gordon, J. S. Binkley, J. A. Pople, W. J. Pietro and W. J. Hehre, *J. Am. Chem. Soc.*, 1982, **104**, 2797–2803.
60 W. J. Pietro, M. M. Francl, W. J. Hehre, D. J. DeFrees, J. A. Pople and J. S. Binkley, *J. Am. Chem. Soc.*, 1982, **104**, 5039–5048.
61 K. D. Dobbs and W. J. Hehre, *J. Comput. Chem.*, 1986, **7**, 359–378.
62 K. D. Dobbs and W. J. Hehre, *J. Comput. Chem.*, 1987, **8**, 861–879.
63 K. D. Dobbs and W. J. Hehre, *J. Comput. Chem.*, 1987, **8**, 880–893.
64 N. M. O'boyle, A. L. Tenderholt and K. M. Langner, *J. Comput. Chem.*, 2008, **29**, 839–845.